

Modeling and Simulation of a Long-Wave Infrared Polarimetric Sensor for Space Object Detection and Characterization

Kevin Pohl, Jonathan Black, Jonathan Pitt, Edward Colbert
Virginia Polytechnic Institute and State University
900 N Glebe Rd, Arlington, VA, 22203; 443-540-0288
kpohl@vt.edu

ABSTRACT

Long-Wave Infrared (LWIR, wavelength $> 8 \mu\text{m}$) polarimetric measurements can be used to characterize space objects. A simulation of a sensor for collection of LWIR polarimetric signatures of space objects has been assembled using two software packages: MATLAB, and FRED. A statistical approach developed for unresolved visible light polarimetric observations of GEO satellites has been adapted for unresolved LWIR polarimetric observations of LEO satellites, showing both that well-known objects can be recognized and anomalies--for example, a major change in shape due to the presence in the scene of another object--can be detected. Though the satellites are effectively point sources, the aggregate polarization values across many measurements can be used to differentiate objects of different shape and material composition.

INTRODUCTION

The objective of the project, a part of which is documented here, is to explore a new avenue for space situational awareness (SSA). Today, SSA is maintained through a combination of ground sensors (radars, telescopes) and voluntary sharing of telemetry and other information with various organizations that maintain active catalogs of space objects^{1,2}. The present work seeks to demonstrate, initially through modeling and simulation, the characterization of low Earth orbit (LEO) satellites by a long-wave infrared polarimetric imaging system.

Passive long-wave infrared polarimetry for man-made object detection has been the subject of numerous studies since at least the 1990s^{3,4,5}. The advantage of long-wave infrared for these purposes is that it measures primarily the target's self-emission, though emission by nearby sources (e.g. low clouds), and thus reflection off the target, can interfere. This occurs because the reflected light is polarized perpendicularly to the emitted light, resulting in reduced values for S_1 and S_2 ^{5,6}, and thus a reduced signal-to-noise ratio. For space object detection this is not a concern, as space objects are generally not close to each other, and solar radiation incident on the target (and resulting reflected radiation) in the 8.2-9.2 micron band is an order of magnitude or more less than the self-emission of the target. Moreover, there are few, if any, competing background sources of polarized thermal emissions in space. The primary polarized emission sources are interstellar dust particles emitting in the 10+ micron range⁷.

There has also been some work done concerning long-wave infrared (without polarization) for detection of

space objects, beginning in the late 1980s. Targets included geosynchronous satellites, which could be detected but not resolved^{8,9,10}. Studies have also been conducted using space based LWIR sensors to detect and characterize space objects¹¹. In both cases detection was feasible during both daytime and nighttime. Another more recent study concluded that a moderate aperture telescope system would suffice to detect unresolved LEO objects using modern LWIR detectors¹². The tradeoff between visible light collection and LWIR is one of resolution against collection opportunities. When using a long-wave IR sensor, the target is its own source of illumination, where a visible light sensor requires an external source of illumination (e.g. the Sun). However, for equivalent optical system, the spatial resolution of the LWIR sensor is going to be about 18x coarser than that of a visible light sensor.

Long-wave infrared polarimetry has been demonstrated for man-made object detection in a variety of terrestrial and maritime settings^{3,4,13}. In addition, visible spectrum polarimetry has been demonstrated for detection and identification of satellites in geosynchronous orbit GEO^{14,15}. Speicher used visible light polarimetry to detect and identify GEO satellites. The experimental setup only measured S_0 and S_1 , and due to the dimness of the targets required an integration time of ~20 seconds. Repeated observations over time revealed differences in signature between individual satellites, both between different types of vehicles, and between vehicles of the same design, but of different age. The latter effect is of particular interest, as it is the material properties of the surface layer (e.g. paint) that drive the complex index of refraction and thus the polarization

signature⁴. Those material properties change over time due to exposure to the space environment¹⁵. Further work has shown that the superposition of polarization signatures of individual components (e.g. dish antenna, bus, solar panels) creates a composite signature for unresolved objects¹⁶, and that statistical measures can be used to tell objects apart¹⁷.

Fundamentally, the polarization state of a light beam can be described by the Stokes vector \mathbf{S} . The Stokes vector is based on six flux measurements using ideal polarizers in front of a radiometer: horizontal (P_H), vertical (P_V), diagonal (45 and 135 degrees; P_{45} and P_{135} , respectively), and left (P_L) and right circular (P_R)¹⁸. The Stokes vector is then defined as

$$\mathbf{S} = \begin{bmatrix} s_0 \\ s_1 \\ s_2 \\ s_3 \end{bmatrix} = \begin{bmatrix} P_H + P_V \\ P_H - P_V \\ P_{45} - P_{135} \\ P_R - P_L \end{bmatrix} \quad (1)$$

where s_0 , s_1 , s_2 , and s_3 are the Stokes vector components in units of watts per meter squared. The Stokes vector represents an average over area, solid angle, and wavelength¹⁸. From the Stokes vector four common polarization parameters can be determined¹⁹:

$$\text{Flux} \quad P = s_0 \quad (2)$$

$$\text{Degree of polarization} \quad \text{of} \quad DOP = \frac{\sqrt{s_1^2 + s_2^2 + s_3^2}}{s_0} \quad (3)$$

$$\text{Degree of linear polarization} \quad DOLP = \frac{\sqrt{s_1^2 + s_2^2}}{s_0} \quad (4)$$

$$\text{Degree of circular polarization} \quad DOCP = \frac{s_3}{s_0} \quad (5)$$

The bulk of the materials encountered—dielectrics, metals, and thin films (coatings, paints)—have negligible rates of circular polarization¹⁸, reducing the value of DOP and DOCP measurements. While DOLP plays a major role in detecting man-made objects in maritime and terrestrial scenes and can serve the same purpose in a space object detection scheme, it can only provide an indication of the presence of an object. To take a step further and identify that object one needs to consider the elements of the Stokes vector, particularly s_0 , s_1 , and s_2 .

In a series of papers^{16,17}, Beamer, Abeywickrema, and Banerjee demonstrated polarimetry as a useful tool in differentiating space objects from one another, especially unresolved objects. They found that the bulk of optical approaches to space object detection and characterization focused on spectral characteristics

(wavelength and intensity), with only a small proportion investigating polarimetry, and primarily in the visible portion of the spectrum. Polarimetry enables discernment of man-made objects from natural background, because target qualities, such as sharp edges and regular surfaces lend themselves to polarimetric study. Measurements were made in a laboratory environment using a collimated broadband visible spectrum light source and a detector with a wire grid polarizer and a quarter wave plate to determine the Stokes vector parameters. Experiments included moderately complex target geometries resembling simple spacecraft: bus, solar panel, dish antenna¹⁷.

Adapting the work of both Beamer et al.¹⁷ and Dao et al.²⁰, polarization signatures can be investigated in a manner analogous to Johnson photometry, which introduces a set of color spaces based on the relative intensity of four color bands (Blue, Visible, Red, Infrared): B-V, B-R, B-I, V-R, V-I, R-I. Here then the four Stokes parameters S_0 , S_1 , S_2 , S_3 , can also be paired into six unique color spaces: S_1/S_0 , S_2/S_0 , S_3/S_0 , S_2/S_1 , S_3/S_1 , and S_3/S_2 . Given the much lower intensity of circularly polarized light in most circumstances^{16,18}, the terms involving S_3 are dropped. This approach then yields three polarization vector-vector spaces: S_2/S_0 vs. S_1/S_0 , S_2/S_1 vs. S_1/S_0 , and S_2/S_1 vs. S_2/S_0 . Multiple observations of each object from different angles are plotted on a 2-D graph, along with the mean position on the plot for each object. Using a non-Euclidean distance measure, the distance between the mean positions of the observation clusters of different objects can be determined. This distance is a measure for how different one object, i.e. one set of measurements, is from another in polarization space¹⁶.

Some early work used the Mahalanobis distance¹⁶, which focuses on the distance between the mean points of two distributions and considering the average covariance of the two distributions. However, it is better suited to comparison of individual points with a distribution, rather than comparison of two distributions to each other. A more suitable measure is the Bhattacharyya distance (BD), which incorporates a modified Mahalanobis distance in its first term, but whose second term gives additional weight to the covariances of each distribution²⁰:

$$BD = \frac{1}{8} (\bar{\mu}_1 - \bar{\mu}_2)^T \left(\frac{\bar{\Sigma}_1 + \bar{\Sigma}_2}{2} \right)^{-1} (\bar{\mu}_1 - \bar{\mu}_2) + \frac{1}{2} \ln \left(\frac{|\bar{\Sigma}_1 + \bar{\Sigma}_2|}{2 \cdot \sqrt{|\bar{\Sigma}_1| \cdot |\bar{\Sigma}_2|}} \right) \quad (6)$$

In the last term on the right hand side of equation (6), $|\bar{\Sigma}_n|$ is the Frobenius norm of the matrix $\bar{\Sigma}_n$. The

Frobenius norm is used instead of the determinant, because the former gives a better estimate of the maximum excursion of a vector during a linear transformation using the matrix, even if the determinant of the matrix is zero²¹. $\bar{\mu}_1 = (x_{\mu 1}, y_{\mu 1})$ is the mean vector of the first class of vectors $\bar{V}_1 = \{x_{i1}, y_{i1}\}$ being compared, and $\bar{\mu}_2 = (x_{\mu 2}, y_{\mu 2})$ is the mean vector of the first class of vectors $\bar{V}_2 = \{x_{i2}, y_{i2}\}$, each representing the “center of mass” of its respective distribution¹⁷. $\bar{\Sigma}_1$ and $\bar{\Sigma}_2$ are the 2×2 covariance matrices of the measurement vectors \bar{V}_1 and \bar{V}_2 , respectively.

TOOLS

Optical Photonics: FRED

FRED Optical Engineering Software simulates the propagation of light through any optomechanical system by raytracing. It provides a multitude of design and analysis tools and is used across a broad set of applications, including stray light analysis, lasers, imaging systems and non-imaging optics, and thermal imaging. FRED enables rapid virtual prototyping and real-time visualization and editing of complex optical systems. It also accurately simulates virtually any type of light source. Finally, it allows for detailed surface definitions, including different materials, scatter models, and thin film coatings²².

Data processing: MATLAB

MATLAB was developed in the 1970s as a linear algebra tool, written in Fortran. It could perform a limited number of functions and had some ability to output graphics. By the early 1980s it had been ported to C with expanded functionality and a more user-friendly interface. It was rolled out as a commercial product by MathWorks in 1984²³. Since then, The core functionality has been further expanded with dozens of tool boxes for everything from signal processing and image processing to control systems to statistics and optimization, and more²⁴. The primary MATLAB functionality used in this research is array manipulation. MATLAB readily ingests the text files generated by FRED and reconditions the data for use in Excel for visualization purposes.

MODELING AND SIMULATION

In earlier work presented elsewhere, satellites of different shape and material composition were compared both in the visible spectrum and in LWIR. These initial simulations provided a baseline for the magnitude of the statistical distances between different vehicles²⁵.

Of particular importance to the present research is FRED’s ability to keep track of the polarization state of the rays through the entire optomechanical model and its flexibility in defining light sources. In the situations modeled here, it is the satellites themselves that act as light sources in the thermal infrared (above $8 \mu\text{m}$ wavelength). The polarization of the emitted light is a function of the surface properties of the satellite: materials and thin film coatings (e.g paint). Likewise, the amount of thermal radiation emitted is a function of those same surface properties.

In FRED materials and coatings are defined by material properties. There are many ways to define the optical properties of materials, but the method chosen here was to provide wavelength dependent values for the complex index of refraction, the reflectance, and transmittance for each material used. FRED itself performs evaluations of the Fresnel equations at each interface and keeps track of the changes in polarization state of each ray generated. The light sources generate light rays with random polarization—collectively this makes for unpolarized light. Their interaction with the vehicles’ surfaces then results in a preferential polarization direction.

Here the presence of another space object in close proximity to the primary vehicle was studied, using in simulation a setup similar to one that would be used in a lab setting. The primary vehicle was a 1-meter cube, with a large solar panel on top (Figure 1). The secondary vehicle was shaped like a 3U cubesat, but substantially larger with a “wingspan” of 1 meter (Figure 2). The surface colors represent the materials used to represent the vehicle components. Silicon was used for the solar panels (lilac), aluminum (gray) and Kapton (brown) for bus and structure surfaces.

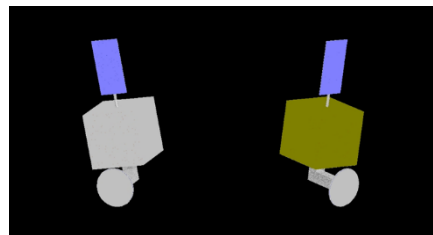


Figure 1: Primary vehicles, aluminum bus (left) and Kapton bus (right)

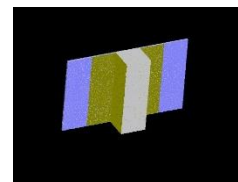


Figure 2: Secondary vehicle

The simulations were run multiple times with two versions of the primary vehicle. The first is almost entirely composed of bare aluminum surfaces, except for its solar panel, the other has a Kapton coating on the major bus surfaces. The secondary vehicle is composed of the same three materials; its configuration was inspired by NASA's ICECUBE cubesat.

Sources were created in the FRED software to represent the emitted light from for each surface. The relevant material constants were culled from various sources and provided to the software, which then used that information to generate polarized rays.

For each primary vehicle the following 10 scenarios were investigated: No secondary, the baseline case; secondary in front of primary, above primary, and off to one side, but fully visible when viewed from the front; secondary slightly behind the primary and partially obscured when viewed from the front, with obscuration varying from 25% to 90%.

The sensor started at a position -30 degrees from the center line and was rotated in one-degree increments to +30 degrees from the centerline. At each position a polarimetric measurement was taken and stored to a file. In all ten files were produced, one for each scenario. Each file contains the measured values for S_0 , S_1 , S_2 . Using a set of MATLAB scripts, the data from each scenario were first processed to add calculated values for S_1/S_0 , S_2/S_0 , and S_2/S_1 , all normalized for better comparability. Then they were compared to the baseline case (no secondary vehicle).

The processed data yielded three graphs per pair of scenario, one for each of the vector-vector spaces investigated (S_2/S_0 vs. S_1/S_0 , S_2/S_1 vs. S_1/S_0 , and S_2/S_1 vs. S_2/S_0). Each graph shows the distribution of measurement points, as well as the mean point (center of gravity) of the distribution for each distribution. In addition to the graphical representation, the Bhattacharyya distance was determined for each pair of vehicles (e.g. vehicle 1a vs. vehicle 2a, etc.). Figures 3 through 6 provide some representative examples of the distributions encountered.

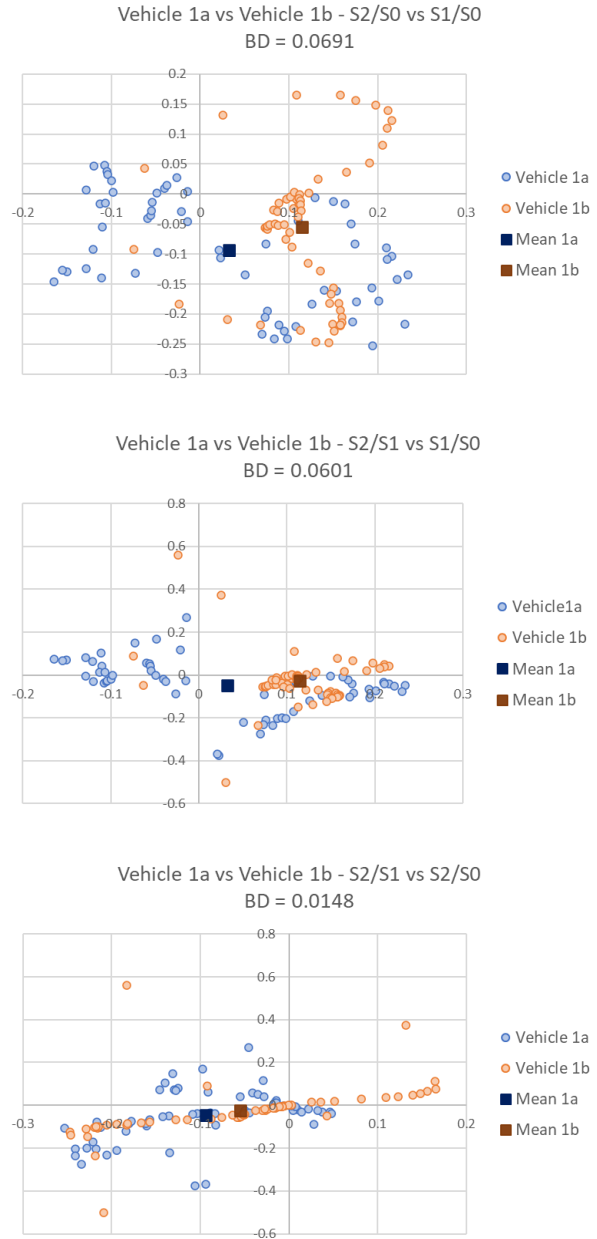


Figure 3: Comparison of baseline cases: Kapton bus (Vehicle 1a) vs. aluminum bus (Vehicle 1b) for all three vector-vector space comparisons

The BD between vehicles of the same shape but different materials is on the order of 10^{-2} . The BD for vehicles of different shape, but same materials is similar.

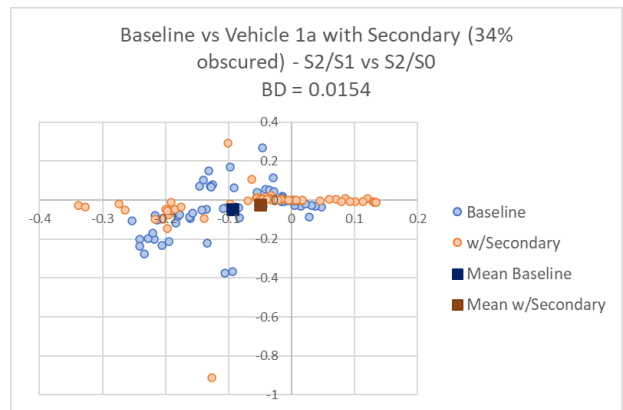
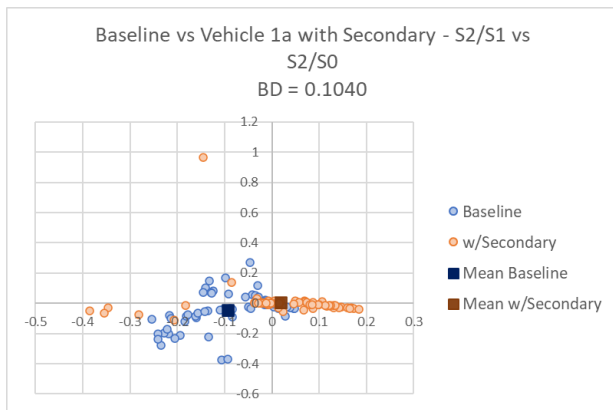
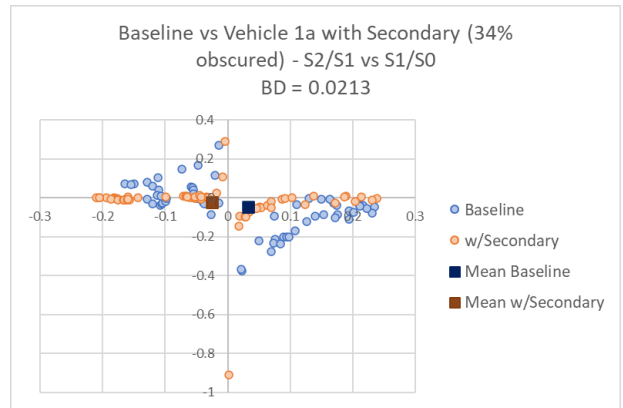
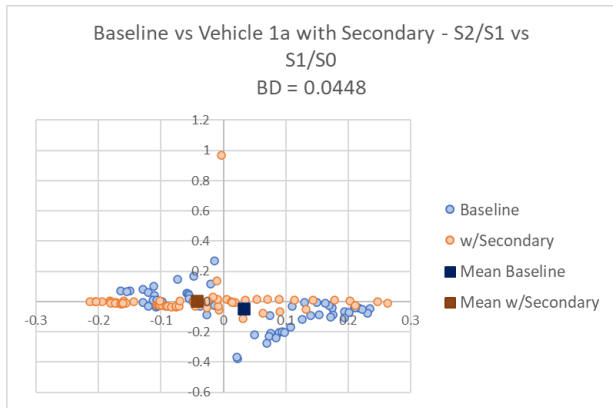
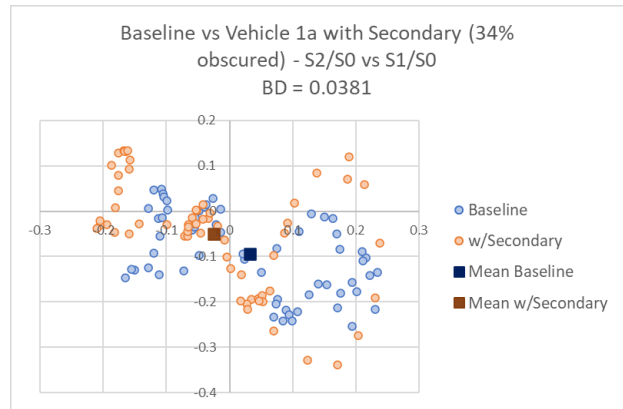
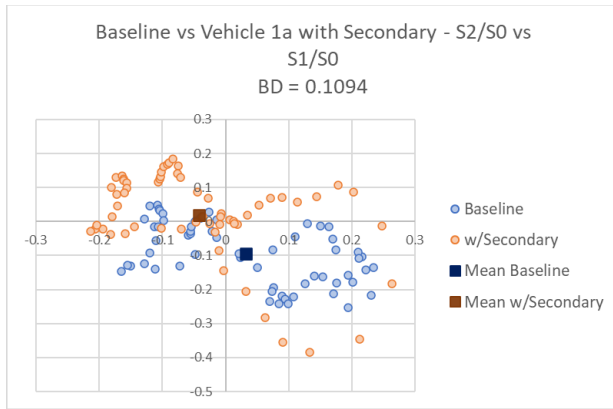


Figure 4: Comparison of baseline case (Kapton bus: Vehicle 1a) vs. Vehicle 1a with the secondary vehicle directly in front for all three vector-vector space comparisons

Figure 5: Comparison of baseline case (Kapton bus: Vehicle 1a) vs. Vehicle 1a with the secondary vehicle partially obscured (34% obscuration when viewed from the front) for all three vector-vector space comparisons

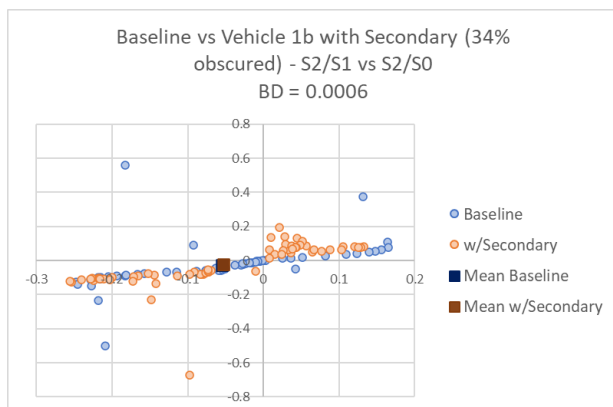
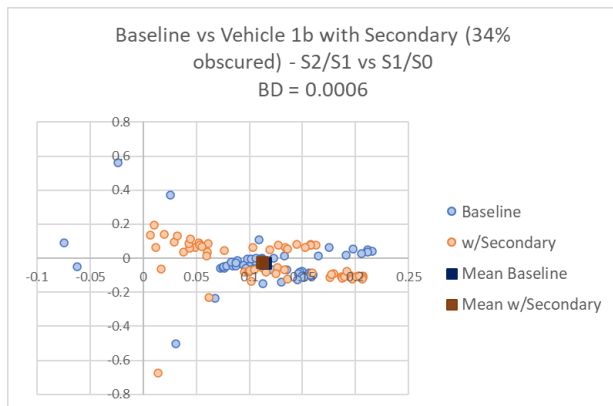
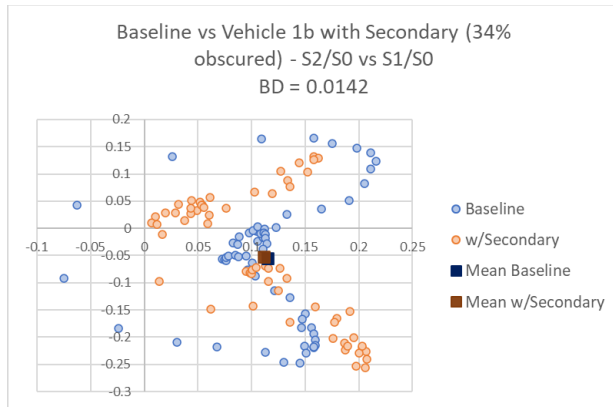


Figure 6: Comparison of baseline case (Aluminum bus: Vehicle 1b) vs. Vehicle 1b with the secondary vehicle partially obscured (34% obscuration when viewed from the front) for all three vector-vector space comparisons

As can be seen, the BD values also differ with different relative positions of the secondary vehicle, as well as with the material composition of the vehicles. Note the sharp reduction in BD when going from Vehicle 1a (Kapton) to Vehicle 1b (Aluminum). There is more signal (i.e. more strongly linearly polarized light) coming from the aluminum bus, resulting in smaller difference between the baseline measurement and the

measurement with the secondary object in the scene, but partially obscured.

CONCLUSIONS

This method has potential in that it allows the discrimination between a known object and that same object with something else nearby in certain circumstances. However, a sufficient amount of the secondary object must be visible in order to detect a difference. Depending on material composition one the other object may be emitting substantially more strongly polarized light than the other. If this is the primary vehicle, then it can be difficult to detect a secondary object nearby.

For geosynchronous applications this would be problematic, as the scene diversity (viewing angle of the targets) from a given ground site is very limited by the nature of the orbit. For low Earth orbit applications, this is likely not as much of a problem. The vehicle and its secondary object will be viewed from different angles throughout an orbital pass and from pass to pass, resulting in one or more collections where the secondary vehicle is more clearly visible.

An anomaly detection system based on this approach would benefit greatly from having a large number of collection locations to ensure a wide diversity of views of a particular space vehicle.

REFERENCES

1. 18 SPCS, 13 February 2018. [Online]. Available: <https://twitter.com/18SPCS/status/963629809921351680>. [Accessed 31 October 2019].
2. Air University, "Space Surveillance," United States Air Force, [Online]. Available: <http://www.au.af.mil/au/awc/awcgate/usspcfs/space.htm>. [Accessed 13 July 2019].
3. K. Gurton, M. Felton, R. Mack, D. LeMaster, C. Farlow, M. Kudenov and L. Pezzaniti, "MidIR and LWIR Polarimetric Sensor Comparison Study," in *Proceedings of SPIE Defense, Security and Sensing*, Orlando, 2010.
4. D. Lemaster and M. Eismann, "Passive Polarimetric Imaging," in *Multi-Dimensional Imaging*, John Wiley & Sons, 2014.
5. T. J. Rogne, F. G. Smith and J. E. Rice, "Passive Target Detection Using Polarized Components of Infrared Signatures," in *Proceedings of Polarimetry '90*, Huntsville, 1990.
6. D. Wellems, S. Ortega, D. Bowers, J. Boger and M. Fetrow, "Long Wave Polarimetric Model: Theory, Measurements, and Parameters," *Journal*

- of Optics A: Pure and Applied Optics*, vol. 8, September 2006.
7. J. Tinbergen, *Astronomical Polarimetry*, Cambridge: Cambridge University Press, 1996.
 8. C. J. Baddiley, "The Potential of CdHgTe Staring Array Infrared Detectors for Satellite Detection," in *Proceedings of Optical Systems for Space and Defence*, London, 1990.
 9. W. P. Seniw, "LWIR Observations of Geosynchronous Satellites," in *Proceedings of the 1993 Space Surveillance Workshop*, Lexington, 1993.
 10. J. K. Lee and D. L. Nishimoto, "Infrared Detection of Geosynchronous Objects at AMOS," in *Proceedings of the 1993 Space Surveillance Workshop*, Lexington, 1993.
 11. P. D. McCall and M. L. A. M. Naudeau, "Debris Characterization Techniques Via Unresolved Long-Wave Infrared Imaging from a Space Platform," *Journal of Applied Remote Sensing*, vol. 8, no. 1, May 2014.
 12. M. R. Hawks and B. J. Steward, "Telescope parameter trade studies for LWIR camera," Air Force Institute of Technology, Wright-Patterson Air Force Base, 2017.
 13. K. Gurton, R. Dahmani and G. Videen, "Measured Degree of Polarization for a Variety of Thermal Emitting Surfaces," Army Research Laboratory, Adelphi, 2004.
 14. A. Speicher, M. Martin, R. Tippets and F. Chun, "Calibration of a System to Collect Visible-Light Polarization Data for Classification of Geosynchronous Satellites," in *Proceedings of SPIE Optical Engineering + Applications*, San Diego, 2014.
 15. A. Speicher, "Identification of Geostationary Satellites Using Polarization Data from Unresolved Images," Denver, 2015.
 16. D. K. Beamer, U. Abeywickrema and P. P. Banerjee, "Polarization Vector Signatures for Target Identification," in *Proc. SPIE 10407, Polarization Science and Remote Sensing VIII*, San Diego, 2017.
 17. D. K. Beamer, U. Abeywickrema and P. P. Banerjee, "Statistical Analysis of Polarization Vectors for Target Identification," *Optical Engineering*, vol. 57, no. 5, May 2018.
 18. R. A. Chipman, "Polarimetry," in *Handbook of Optics*, vol. II, New York, McGraw-Hill, 1995.
 19. R. M. Azzam and N. M. Bashara, *Ellipsometry and Polarized Light*, Amsterdam: North-Holland Publishing Company, 1977.
 20. P. D. Dao, P. J. McNicholl, J. H. Brown, J. E. Cowley, M. J. Kendra, P. N. Crabtree, A. V. Dentamaro, E. V. Ryan and W. Ryan, "Space Object Characterization with 16-Visible-Band Measurements at Magdalena Ridge Observatory," Defense Technical Information Center, 2008.
 21. C. D. Meyer, *Matrix Analysis and Applied Linear Algebra*, Philadelphia: Society for Industrial and Applied Mathematics, 2000.
 22. Photon Engineering, LLC, "What is FRED?," [Online]. Available: <https://photonengr.com/fred-software/>. [Accessed 21 August 2019].
 23. C. Moler, "The Origins of MATLAB," 2004. [Online]. Available: <https://www.mathworks.com/company/newsletters/articles/the-origins-of-matlab.html>. [Accessed 3 January 2020].
 24. C. Moler, "A Brief History of MATLAB," 2018. [Online]. Available: <https://www.mathworks.com/company/newsletters/articles/a-brief-history-of-matlab.html>. [Accessed 3 January 2020].
 25. K. Pohl, J. Black, J. Pitt and E. Colbert, "Low Earth orbit space object differentiation using long-wave infrared polarimetry," in *Proc. SPIE 11412, Polarization: Measurement, Analysis, and Remote Sensing XIV*, Anaheim, 2020.